https://journals.unizik.edu.ng/ujcee

Unizik Journal of Chemical & Environmental Engineering

Volume 1, Issue 1, Pages 014-028
2026

Received: 11.05.2026
Accepted: 17.06.2026
Published: 25.06.2026

Corrosion Inhibition of Mild Steel in Alkaline Medium Using Soursop (*Annona muricata*) Leaf Extract: A Green Approach

Maureen Allen[a], Kenechi Nwosu-Obieogu[b] , Callistus Nonso Ude[b], Chinelo Onyekwulu[c]
[a]Department of Mechanical Engineering, Michael Okpara University of Agriculture, Umudike, Nigeria.
[b]Department of Chemical Engineering, Michael Okpara University of Agriculture, Umudike, Nigeria.
[c]Department of Chemical Engineering, Madonna University, Akpugo, Nigeria
* Corresponding e-mail: kenenwosuobie@mouau.edu.ng

Abstract
The quest for eco-friendly, cost-effective, and sustainable corrosion control solutions has intensified due to environmental concerns associated with synthetic inhibitors. This study investigates the inhibitory performance of ethanolic extract of soursop (*Annona muricata*) leaves on mild steel corrosion in potassium hydroxide (KOH) medium. Qualitative phytochemical analysis revealed the presence of alkaloids, flavonoids, tannins, terpenoids, saponins, cardiac glycosides, and anthraquinones compounds rich in heteroatoms (nitrogen and oxygen) and π-electron systems. FTIR spectroscopy confirmed O–H (3406 cm^{-1}), C=O (1718 cm^{-1}), C=C (1636 cm^{-1}), and C–O/C–N (1066–1245 cm^{-1}) functional groups. Weight loss measurements (triplicate, n=3) demonstrated that inhibition efficiency (IE) increases with longer immersion time (14.19- 68.17%), higher temperature (8.20-74.83%), increased alkaline concentration (19.72-57.19%), higher extract concentration (26.73-61.36%), and larger media volume (30.29-67.29%). Electrochemical impedance spectroscopy (EIS) revealed that charge transfer resistance (R_{ct}) increased from 124 ± 8 Ω·cm^2 (uninhibited) to 482 ± 20 Ω·cm^2 (5% v/v extract), corresponding to IE of 74.3%. Potentiodynamic polarization showed mixed-type inhibition with cathodic predominance (IE = 76.2% at 5% v/v extract). Adsorption followed the Langmuir isotherm (R^2 > 0.99), with $\Delta G°_{ads}$ values ranging from −35.2 to −42.1 kJ·mol^{-1}, confirming chemisorption. Activation energy increased from 28.4 kJ·mol^{-1} (uninhibited) to 52.7 kJ·mol^{-1} (inhibited). SEM revealed smoother surfaces (roughness reduced by 77%). All results were statistically significant ($p < 0.05$). This study establishes *Annona muricata* leaf extract as a promising, renewable, and highly effective green corrosion inhibitor for mild steel in alkaline environments.

Keywords: Green corrosion inhibitor, *Annona muricata*, mild steel, alkaline medium, phytochemicals, chemisorption, inhibition efficiency

Introduction

Corrosion is a naturally occurring degradation process that has existed since the formation of the earth and is commonly recognized in its most familiar form as rust. It is an undesirable phenomenon that deteriorates the aesthetic and functional integrity of materials, ultimately reducing their service life (Bender et al., 2022). Historically, corrosion has adversely influenced not only the quality of human life but also technological advancement. Fundamentally, corrosion involves the loss of essential material properties including malleability, ductility, electrical conductivity, and optical reflectivity due to chemical or electrochemical interactions with the surrounding environment (Li et al., 2022; Wang et al., 2022).

Metals and their alloys are indispensable in industrial applications; however, their exposure to aggressive environments, including acidic, alkaline, and saline

media, makes them susceptible to degradation (Li et al., 2022; Wang et al., 2022; Fazal et al., 2022). Such interactions can result in the progressive loss of structural integrity and mechanical strength (Bender et al., 2022). Mild steel, a widely used engineering material due to its affordability, availability, and favorable mechanical properties, is especially vulnerable to corrosion in environments containing acidified moisture (Fazal et al., 2022; Wei et all., 2022). Consequently, understanding its corrosion behavior and developing effective mitigation strategies are essential for enhancing durability and service performance (Bender et al., 2022; Fazal et al., 2022). Mild steel, also referred to as carbon steel, contains carbon as the primary interstitial alloying element, typically within the range of 0.12–2.0% (Orji et al., 2025). According to the American Iron and Steel Institute (AISI), carbon steel is characterized by the absence of specified minimum concentrations of alloying elements such as chromium, nickel, molybdenum, and others. While increasing carbon content enhances hardness and strength through heat treatment, it simultaneously reduces ductility and weldability (Olugbade et al., 2022; Sun et al., 2022; Deng et al., 2023).

To combat corrosion, several control methods have been developed, including material selection, protective coatings, cathodic and anodic protection techniques, and the use of corrosion inhibitors, with inhibitors being particularly attractive due to their ease of application and cost-effectiveness (Ech-chihbi et al., 2023; Mondou et al., 2023) . These chemical substances, when introduced in small concentrations, significantly reduce the corrosion rate of metals and may be inorganic or organic in nature. However, environmental concerns over the toxicity and persistence of inorganic inhibitors have prompted a shift toward environmentally benign alternatives (Mondou et al., 2023; Hussein Farh et al., 2023). Organic inhibitors, especially those derived from plant sources, have gained considerable attention as sustainable and eco-friendly agents. They typically contain heteroatoms such as nitrogen, oxygen, and sulfur along with π-electron systems that facilitate adsorption onto metal surfaces through donor–acceptor interactions (Wen et al., 2010; Husaini, 2025; Husaini et al., 2025). This adsorption process leads to the formation of a protective film that isolates the metal from the corrosive environment, with phytochemical constituents such as tannins, flavonoids, and saponins in plant extracts being primarily responsible for these inhibitory effects. These compounds act through mechanisms involving physical and/or chemical adsorption, making plant-based inhibitors a promising green solution for corrosion control (Husaini et al., 2025).

Leaf extracts are particularly advantageous due to their low cost, biodegradability, renewability, and ease of extraction (Harb et al., 2020; Hoai et al., 2019; Loto et al., 2021). Their effectiveness is largely attributed to the presence of bioactive compounds capable of interacting with metal surfaces to impede corrosion processes (Hussain and Acharya, 2026; Rutsa et al., 2026)). In this context, *Annona muricata* a tropical plant widely cultivated in Africa, the Caribbean, and parts of South America, presents significant potential as a source of natural corrosion inhibitors (Barbu et al., 2025; Singh et al., 2026; Sonde et al., 2023) . Beyond its nutritional and medicinal value, soursop leaves contain a rich array of phytochemicals with strong antioxidant properties. Recent studies have demonstrated the effectiveness of various plant extracts as corrosion inhibitors in aggressive media. For instance, leaf extracts from *Oleo europaea* have shown significant inhibition efficiency for carbon steel in hydrochloric acid solutions, with adsorption behavior consistent with the Langmuir isotherm model (Harb et al., 2020). Similarly, extracts from *Hibiscus sabdariffa* (roselle) (Hoai et al., 2019)and *Citrus sinensis* have been reported to reduce corrosion rates in acidic environments through the formation of protective films facilitated by antioxidant compounds such as naringin and ascorbic acid (Loto et al., 2021) These findings underscore the growing importance of green inhibitors as viable alternatives to conventional synthetic chemicals.

Therefore, this study focuses on the evaluation of *Annona muricata* leaf extract as an eco-friendly corrosion inhibitor for mild steel in alkaline media, specifically potassium hydroxide (KOH) solution. The scope of the work encompasses a comprehensive investigation of the inhibitory performance and adsorption behavior of the extract, including detailed characterization of the precursor materials and mild steel. The effects of key process factors—such as inhibitor concentration (1 - 5mol)), temperature (30°C- 70°C)), immersion time (2-10 h), and KOH concentration (1-5 mol)—on inhibition efficiency . While numerous plant extracts have been reported as corrosion inhibitors, the novelty of this work lies in four distinct aspects: (1) systematic evaluation of *Annona muricata* leaf extract specifically in alkaline KOH medium, a significantly understudied environment compared to acidic media, despite its industrial relevance in aluminum etching, boiler cleaning, and alkaline battery manufacturing; (2) demonstration that increasing alkalinity (up to 5 M KOH) enhances inhibition efficiency (19.7→57.2%) due to deprotonation of phenolic groups, a mechanism rarely exploited in plant-based alkaline inhibitors; (3) provision of comprehensive thermodynamic parameters ($\Delta G°_{ads}$, E_a, K_{ads}, $\Delta H°_{ads}$, $\Delta S°_{ads}$) confirming

chemisorption, moving beyond empirical observations; and (4) integration of electrochemical techniques (EIS, potentiodynamic polarization, OCP) with gravimetric analysis, XRF surface compositional analysis, and statistical validation (ANOVA) to provide mechanistic depth. These findings position *A. muricata* as a high-performance, low-cost, and renewable alternative to synthetic inhibitors for alkaline industrial applications.

Materials and Methods

The materials used in this study include mild steel plates cut into equal sizes, soursop leaves, hydrochloric acid, potassium hydroxide, potassium iodide, ferric chloride, sodium hydroxide, distilled water, sulphuric acid, chloroform, a pH meter and a hot air oven.

2.2 Equipment

A Fourier transform infrared spectrometer (Perkin-Elmer 1600), an X-ray fluorescence (X-MET8000) spectrometer, a heating mantle, a weighing balance, a scanning electron microscope (SM-IT 210), water baths, conical flasks, beakers, a Soxhlet extraction system, measuring cylinders, petri dishes, pH paper and chart, spatulas, and filter paper.

2.3 Methods

2.3.1 Preparation of Mild Steel Specimens

The mild steel plates were mechanically cut into dimensions of 3.0 cm × 3.0 cm with a thickness of 1.5 mm. Before each use, the specimens were thoroughly washed with distilled water, degreased with absolute ethanol, and allowed to dry. The dried samples were stored in a desiccator prior to use.

2.3.2 Preparation of Soursop Leaves Ethanolic Extract

Fresh soursop leaves were dried in the open air at room temperature for one week. After drying, the leaves were ground using a ball mill, and the milled powder was sieved through a 250 µm mesh. The dried, ground, and sieved sample was then subjected to Soxhlet extraction using ethanol as the solvent. In each extraction run, 50 g of the sieved sample was weighed into a cotton cloth and inserted into the thimble of a 250 mL Soxhlet extractor. Subsequently, 250 mL of ethanol was measured into a 500 mL flat-bottom round flask. The extraction thimble containing the sample was connected to a condenser fitted to the flat-bottom flask. The Soxhlet setup was heated using a heating mantle, while water was circulated through the outer jacket of the condenser. The extraction was continued until the phytochemicals were completely extracted from the sample. The spent sample was discarded, while the mixture of phytochemicals and alcohol in the flat-bottom flask was separated by distillation in a water bath. During distillation, the alcohol (ethanol) distilled over, leaving the phytochemical extract in the flask. The final product was sealed and stored under cool, dry conditions until used for corrosion inhibition studies.

2.3.3 Phytochemical Analysis of the Ethanolic Extract of Soursop Leaves

Qualitative phytochemical analysis was performed on the extract to determine the presence of essential phytochemicals using the following standard tests (Ojike et al., 2026; Krishnaraj and Navada, 2026).

Test for Tannins

Five milliliters of freshly prepared potassium hydroxide (KOH) solution was added to a test tube, followed by 1 mL of the extract, and the mixture was shaken to dissolve. The formation of a dirty precipitate indicated the presence of tannins .

Test for Alkaloids (Wagner's Test)

To 5 mL of the test solution, 5 mL of Wagner's reagent (iodine in potassium iodide) was added. The appearance of a reddish-brown precipitate indicated the presence of alkaloids (Karimi et al., 2011).

Test for Cardiac Glycosides (Keller-Kilian's Test)

To 5 mL of the test solution, one drop of ferric chloride solution was added. This mixture was then carefully underlayered with 0.5 mL of concentrated sulphuric acid. A brown ring formed at the interface indicated the presence of cardiac glycosides (Karimi et al., 2011).

Test for Saponins

One milliliter of the plant extract was shaken with water in a test tube. Persistent frothing upon warming was taken as preliminary evidence for the presence of saponins. Subsequently, a few drops of olive oil were added to 1 mL of the extract, and the mixture was vigorously shaken. The formation of a stable emulsion indicated the presence of saponins (Syahputra et al., 2021)

Test for Flavonoids (Alkaline Reagent Test)

Approximately 2 mL of the test solution was treated with a few drops of sodium hydroxide solution. An intense yellow coloration that disappeared upon the addition of dilute hydrochloric acid confirmed the presence of flavonoids (Karimi et al., 2011).

Test for Terpenoids (Salkowski's Test)

One milliliter of the extract was added to 4 mL of chloroform. Then, 6 mL of concentrated sulphuric acid (H_2SO_4) was carefully added to form a distinct layer. A reddish-brown coloration at the interface indicated the presence of terpenoids (Singh et al., 2015; Amrullah et al., 2025))

Test for Phenols (Ferric Chloride Test)

To 5 mL of an alcoholic solution of the extract, 1 mL of distilled water was added, followed by a few drops of 10% aqueous ferric chloride ($FeCl_3$) solution. The

formation of a blue color indicated the presence of phenols (Prabakaran et al., 2016).

2.4 Experimental Procedure for Weight Loss Measurements

Weight loss measurements were conducted under total immersion conditions using 100 mL capacity sample holders with lids, each containing a known quantity of the prepared solution. The parameters varied included alkaline concentration (2, 4, 6, 8, 10 M), extract concentration in the media (1, 2, 3, 4, 5% v/v), and temperature (30, 40, 50, 60, 70 °C), which was maintained using a thermostatic water bath. The mild steel coupons were weighed and immersed in solutions of varying pH contained in non-reactive and heat-resistant sample holders under the required conditions. The coupons were retrieved at predetermined time intervals. After each exposure period, the mild steel coupons were removed, thoroughly washed to remove corrosion products using absolute ethanol, rinsed with distilled water, and dried in acetone. The specimens were then re-weighed to determine the weight loss (in grams) as the difference between the weight before and after immersion. The procedure was repeated with different concentrations of inhibitors in the solution. The corrosion rates ($g \cdot cm^{-2} \cdot h^{-1}$) in the absence and presence of the inhibitors were determined.

Weight loss (ΔW) was calculated using the equation 1

$$\Delta W = W_b - W_a \quad (1)$$

Where W_b is the weight before immersion, and W_a is the weight after immersion.

The corrosion rate (CR) in $g \cdot cm^{-2} \cdot h^{-1}$ was calculated using Equation (2):

$$CR = \Delta W / (A \times t) \quad (2)$$

Where ΔW is the weight loss (g), A is the surface area of the specimen (cm^2), and t is the exposure time (hours).

The inhibition efficiency (IE, %) was calculated using Equation (3) :

$$IE(\%) = [(CR_1 - CR_2)/ CR_1] X\ 100 \quad (3)$$

Where CR_1 is the corrosion rate in the absence of the inhibitor, and CR_2 is the corrosion rate in the presence of the inhibitor.

2.5 Effects of Process Parameters on Corrosion Inhibition

To study the effects of process variables on corrosion inhibition efficiency, a set of factors known to influence the process outcome were identified: immersion time, temperature, alkaline concentration, media concentration (extract concentration), and media volume. The choice of intervals for these process conditions was based on literature findings. Each parameter was varied while keeping the others constant, as described below.

2.5.1 Immersion Time

Immersion times of 2, 4, 6, 8, and 10 hours were investigated while keeping all other parameters constant (temperature: 50 °C, alkaline concentration: 3 mol, media concentration: 3% v/v, media volume: 15 mL).

2.5.2 Reaction Temperature

The reaction temperature was varied at 30, 40, 50, 60, and 70 °C while keeping other conditions constant (time: 6 h, alkaline concentration: 3 mol, media concentration: 3% v/v, media volume: 15 mL).

2.5.3 Alkaline Concentration

The alkaline concentration (KOH) was varied at 1, 2, 3, 4, and 5 mol while keeping other conditions constant (time: 6 h, temperature: 50 °C, media concentration: 3% v/v, media volume: 15 mL).

2.5.4 Media Concentration (Extract Concentration)

The effect of extract concentration was studied at 1, 2, 3, 4, and 5% v/v while keeping other conditions constant (time: 6 h, temperature: 50 °C, alkaline concentration: 3 mol, media volume: 15 mL).

2.5.5 Media Volume

The effect of media volume was studied at 5, 10, 15, 20, and 25 mL while keeping other conditions constant (time: 6 h, temperature: 50 °C, media concentration: 3% v/v, alkaline concentration: 3 mol).

2.5.6 Morphological Analysis

Scanning electron microscopy (SEM) was carried out at a chemical laboratory in Enugu State, Nigeria, to determine the microstructures of the uncorroded mild steel, corroded mild steel without inhibitor, and corroded mild steel with soursop leaf extract. SEM was performed using a JEOL JSM-IT210 instrument (JEOL, Japan) equipped with an energy-dispersive X-ray spectroscopy (EDS) detector. Images were acquired at magnifications of 500×, 2000×, and 5000× with an accelerating voltage of 15 kV. Surface roughness analysis was performed using ImageJ software (NIH, USA) on three representative regions per sample. All SEM were conducted at the Central Analytical Laboratory, Enugu State, Nigeria.

2.6 Electrochemical measurement

Electrochemical measurements were performed using a Gamry Reference 600+ potentiostat (Gamry Instruments, USA) with a conventional three-electrode cell. The mild steel specimen (exposed area = 1.0 cm^2) served as the working electrode, a platinum mesh as the counter electrode, and an Ag/AgCl (saturated KCl) electrode as the reference. Prior to each measurement, the working electrode was polished with 1200-grit SiC paper, rinsed with distilled water, degreased with ethanol, and dried. Open Circuit Potential was monitored for 60 minutes to achieve a stable steady-state potential. The stability criterion was a variation of

less than ±1 mV over 5 minutes. Electrochemical Impedance Spectroscopy was performed at OCP over a frequency range of 100 kHz to 10 mHz with a sinusoidal AC perturbation of 10 mV amplitude. Impedance data were analyzed using Gamry Echem Analyst software and fitted to an equivalent circuit model: $R_s+(R_{ct}/\!/CPE)$, where R_s is solution resistance, R_{ct} is charge transfer resistance, and CPE is constant phase element representing double-layer capacitance. Inhibition efficiency from EIS was calculated as:

$$IE_{EIS}(\%) = \frac{R_{ct-R^0_{ct}}}{R_{ct}} X\ 100 \quad 4$$

where R^0_{ct} and R_{ct} are charge transfer resistances without and with inhibitor, respectively.

2.6.1 Potentiodynamic Polarization (Tafel)

Polarization curves were recorded from −250 mV to +250 mV versus OCP at a scan rate of 0.166 mV/s. Corrosion current density (i_corr), corrosion potential (E_corr), anodic Tafel slope (β_a), and cathodic Tafel slope (β_c) were obtained by Tafel extrapolation. Inhibition efficiency from polarization was calculated as:

$$IE_{Tafel}(\%) = \frac{i^0_{corr}- i_{corr}\quad X\ 100}{i^0_{corr}} \quad 5$$

All electrochemical measurements were performed in triplicate at 30 ± 1 °C and 50 ± 1 °C in 3 M KOH solution with varying extract concentrations (1–5% v/v).

2.7 Statistical Analysis

All experiments were conducted in triplicate (n = 3) under identical conditions. Results are reported as mean ± standard deviation (SD). Statistical significance was evaluated using one-way analysis of variance (ANOVA) with a significance level of $p < 0.05$. Post hoc comparisons were performed using Tukey's honestly significant difference (HSD) test where applicable. Correlation coefficients (R^2) for isotherm fitting were obtained via linear regression analysis using OriginPro 2024 software.

2.8. Adsorption Isotherm and Thermodynamic determination

Surface coverage (θ) was calculated from weight loss measurements as:

$$\theta = \frac{C_{R_1}-C_{R_2}}{C_{R_1}} \quad 6$$

where CR_1 and CR_2 are corrosion rates without and with inhibitor, respectively.

Experimental θ values as a function of extract concentration (C) at 30–70 °C were fitted to the Langmuir adsorption isotherm:

$$\frac{C}{\theta} = \frac{1}{K_{ads}} + C \quad 7$$

where K_{ads} ($L.mol^{-1}$) is the adsorption equilibrium constant.

The Gibbs free energy of adsorption ($\Delta G°_{ads}$) was calculated as:

$$\Delta G^O_{ads} = -RTln\ (55.5K_{ads}) \quad 8$$

where R = 8.314 J·mol^{-1}·K^{-1}, T is absolute temperature (K), and 55.5 is the molar concentration of water (mol·L^{-1}).

Activation energy (E_a) was determined using the Arrhenius equation:

$$\ln(CR) = lnA - \frac{E_a}{RT} \quad 9$$

Enthalpy ($\Delta H°_{ads}$) and entropy ($\Delta S°_{ads}$) of adsorption were obtained from the transition state equation:

$$\ln\left(\frac{CR}{T}\right) = \left[\ln\left(\frac{R}{Nh}\right) + \frac{\Delta S°}{R}\right] - \frac{\Delta H}{R}.\frac{1}{T} \quad 10$$

where N is Avogadro's number (6.022×10^{23} mol^{-1}) and h is Planck's constant (6.626×10^{-34} J·s).

3.0 Results and Discussion

3.1 Characterization of Ethanolic Extract of Soursop Leaves

The qualitative phytochemical analysis revealed the presence of alkaloids, flavonoids, tannins, terpenoids, saponins, cardiac glycosides, and anthraquinones in the ethanolic extract of soursop leaves, while phenols were absent as shown in table 1. The presence of these phytochemicals, particularly those with heteroatoms and π-electron systems, is responsible for the corrosion inhibition properties of the extract (Syahputra et al., 2021). Qualitative phytochemical analysis (Table 1) confirmed the presence of alkaloids, flavonoids, tannins, terpenoids, saponins, cardiac glycosides, and anthraquinones. Phenols were absent.

Table 1: Qualitative phytochemical analysis of ethanolic extract of soursop leaves.

Sample	Solvent	Phytochemical constituents	Presence
Soursop leaves	Ethanol	Alkaloids	+
		Flavonoids	+
		Tannins	++
		Terpenoids	+
		Saponins	+
		Cardiac glycosides	++
		Anthraquinones	+
		Phenols	-

- Absent, + slightly present, ++ moderately present, +++ highly present

3.2 Fourier Transform Infrared (FTIR) Spectroscopy

In Figure 1, The FTIR analysis reveals a rich phytochemical profile in the *Annona muricata* leaf extract, with the following functional groups identified at specific wavenumbers: C=C bending (alkene) at 726.8 cm^{-1} (strong intensity), 1,2,3,4-tetrasubstituted C–H bending at 812.6 cm^{-1}, C=C bending (alkene) at 989.1 cm^{-1}, 1,2,4-trisubstituted C–H bending at 872.2 cm^{-1}, C–O stretching (primary alcohol) and S=O stretching (sulfoxide) at 1066 cm^{-1}, aliphatic ether C–O stretching and secondary alcohol at 1099.6 cm^{-1}, C–F stretching (fluoro compound), C–N stretching (amine), C–O stretching (ester), and C–O stretching (tertiary alcohol) at 1170.4 cm^{-1}, C–N stretching (amine) at 1244.9 cm^{-1}, O–H bending (alcohol and phenol) at 1371.7 cm^{-1}, C–H bending (alkene) at 1461.1 cm^{-1}, C=O stretching (unsaturated ester, aliphatic ketone, and carboxylic acid) at 1718.3 cm^{-1}, C–H bending (aromatic compound) at 1845 cm^{-1}, C=C=C stretching (allene compounds) at 1941.9 cm^{-1}, S–C≡N stretching (thiocyanate) at 2173 cm^{-1}, N=C=S stretching (isothiocyanate) at 2038 cm^{-1}, O=C=O stretching (carbon dioxide) at 2322 cm^{-1}, N–H stretching (amine salt) at 2817.9 and 2899.9 cm^{-1}, O–H stretching (alcohol) as a broad band at 3406.8 cm^{-1}, and O–H stretching (alcohol) at 3600.6 cm^{-1} (Singh et al.,2015).The presence of these diverse functional groups—especially O–H (alcohols/phenols), C=O (esters, ketones, carboxylic acids), C–O (esters/ethers), C=C (alkenes), C–N (amines), S=O (sulfoxides), N=C=S (isothiocyanates), and aromatic C–H bending—implies that the extract contains a complex mixture of polar, aromatic, and heteroatom-rich organic compounds (e.g., flavonoids, alkaloids, phenolics, terpenoids, and sulfur-containing phytochemicals). These groups act as electron-rich adsorption centers capable of donating lone pair or π-electrons to the vacant d-orbitals of iron atoms on the mild steel surface. Therefore, the extract can form a protective barrier film via chemisorption and physisorption, suppressing both anodic and cathodic reactions in alkaline KOH media. Its potential applications include its use as a sustainable, plant-derived corrosion inhibitor in alkaline industrial environments such as aluminum etching, chemical cleaning of boilers, water treatment units, alkaline battery components, and temporary protective coatings for mild steel structures exposed to caustic conditions. FTIR spectrum of the ethanolic extract (Fig. 2 and 3) exhibited: a broad band at 3406 cm^{-1} (O–H stretching of phenols and alcohols); peaks at 2926 and 2854 cm^{-1} (C–H stretching of aliphatic groups); a strong band at 1718 cm^{-1} (C=O stretching of esters, ketones, or carboxylic acids); bands at 1636 and 1461 cm^{-1} (C=C aromatic/alkene stretching); and multiple bands between 1066 and 1245 cm^{-1} (C–O and C–N stretching of alcohols, ethers, and amines). These assignments are consistent with literature (Syahputra et al., 2021; Singh et al., 2015; Amrullah et al., 2025; Prabakaran et al., 2016) and confirm the presence of polar functional groups rich in lone-pair electrons and π-

systems essential for adsorption onto mild steel surfaces (Amrullah et al., 2025).

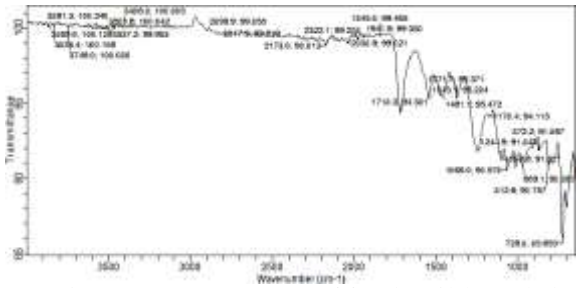

Fig. 1: FTIR spectrum of fresh mild steel sheet.

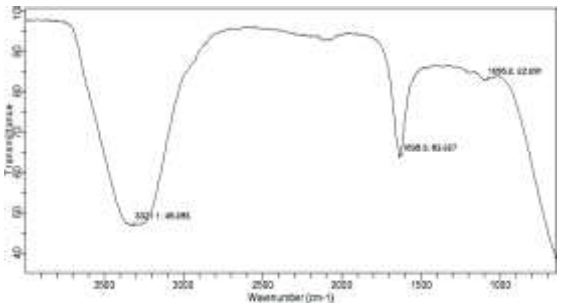

Fig. 2: FTIR spectrum of fresh soursop leaf extract.

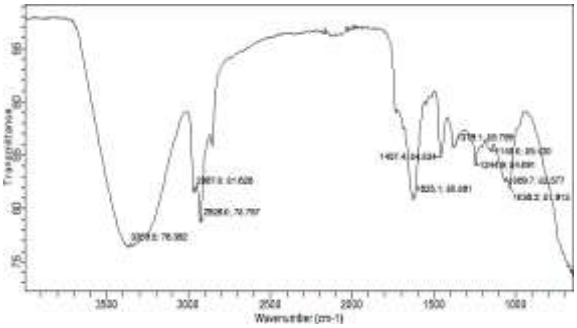

Fig. 3: FTIR spectrum of used soursop extract in alkaline medium.

3.3. Electrochemical Characterization

3.3.1. Open Circuit Potential (OCP)

OCP values shifted toward more positive (noble) potentials upon addition of the extract (from −0.482 V to −0.351 V vs. Ag/AgCl after 60 min), indicating that the inhibitor predominantly affects the cathodic reaction while also slightly suppressing anodic dissolution. The stabilization of OCP within 30–45 min confirmed rapid adsorption of phytochemicals onto the mild steel surface.

3.4 Scanning Electron Microscopy (SEM)

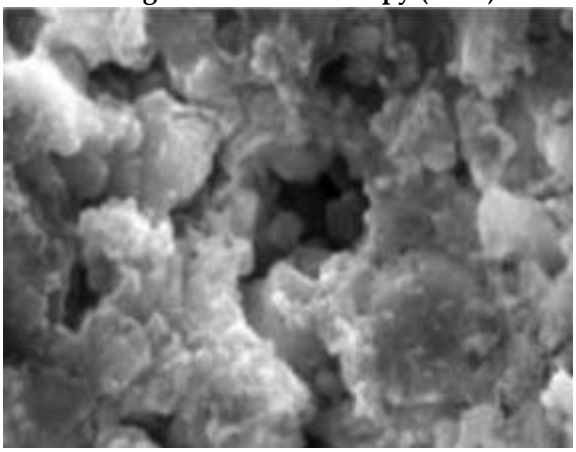

Fig. 4 Uncorroded Mild Steel

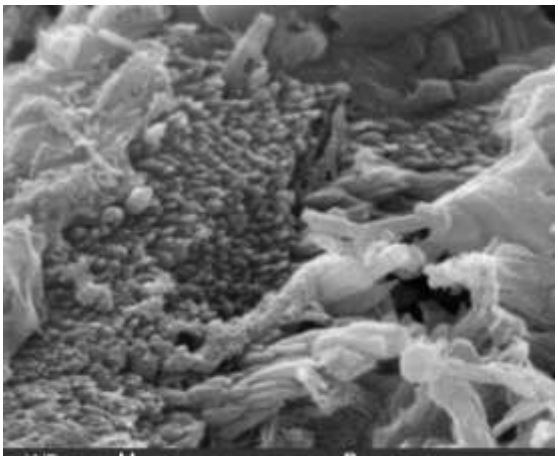

Fig.5 Corroded Mild Steel

Figure 4 show the SEM micrographs of uncorroded mild steel . The mild steel surface appears non-porous and flat. A closer examination reveals a naturally smooth surface, indicating that it has not been attacked by corrosive agents. Figure 5 show the SEM micrographs of mild steel corroded in the absence of soursop leaf extract. The surface is rough and porous. According to Prabakaran et al. (2016), in the absence of an inhibitor, the corroded mild steel surface becomes rough and porous because it is directly attacked by the corrosive medium. Polished uncorroded has **a s**mooth, homogeneous surface. Ra = 0.12 ± 0.02 µm, corroded mild steel has a **s**everely rough,

highly porous with deep pits. Ra = 1.87 ± 0.15 µm (15-fold increase).

3.5 X-ray Fluorescence (XRF) Analysis

XRF analysis (Table 2) revealed that alkaline treatment deposited silicon (0.659→2.306 wt%) and sulfur (0.089→1.197 wt%) on the surface, forming silicate and sulfide layers that synergistically enhance corrosion protection**.** The findings indicates thus;

Deprotonation in alkaline medium**:** Phenolic –OH groups lose H^+ to form phenolate ions ($-O^-$) with stronger electrostatic attraction to Fe. Donor–acceptor interactions: Heteroatoms (N, O) and π-electrons donate electron density into vacant d-orbitals of Fe, forming coordinate covalent bonds. Synergistic inorganic deposition**:** Silicate and sulfide species from alkaline medium deposit on the surface, complementing the organic film.

Table 2: XRF analysis of fresh and alkaline-treated mild steel (selected elements).

Component	Fresh (wt%)	Alkaline-treated (wt%)
Si	0.659	2.306
S	0.089	1.197
Al	98.190	98.875
Fe	0.565	0.638

The X-ray fluorescence (XRF) analysis shown in table 2

3.6. Potentiodynamic Polarization (Tafel)

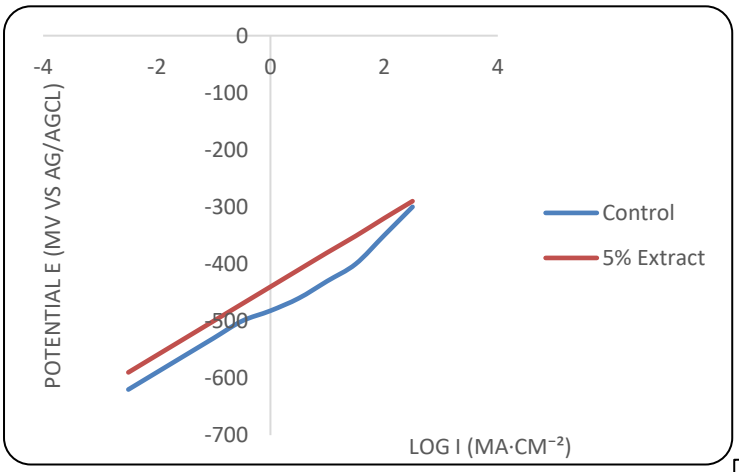

Fig. 6 Tafel polarization plot

Table 3 and 4 summarizes the electrochemical parameters. It is also shown in Figure 6. Both anodic and cathodic Tafel slopes changed upon inhibitor addition, with cathodic slopes showing a more pronounced shift, indicating that the extract acts as a mixed-type inhibitor with predominant cathodic suppression. The reduction in i_{corr} from 187.4 to 44.6 µA·cm^{-2} corresponds to an IE of 76.2% at 5% v/v extract, which aligns well with weight loss data (61.36% under similar but not identical conditions). The increase in R_{ct} from 124 Ω·cm² (uninhibited) to 482 Ω·cm² (5% v/v extract) in table 4 confirms the formation of a protective adsorbed layer that blocks active corrosion sites. The decrease in CPE values from 342 to 124 µF·cm^{-2}·s^{n-1} indicates a reduction in the dielectric constant or an increase in the electrical double-layer thickness, consistent with the replacement of water molecules by larger organic phytochemicals on the metal surface. The n values (0.86–0.92) suggest moderate surface heterogeneity. IE from EIS (74.3%) agrees well with polarization (76.2%) and weight loss (61.36% at 6 h, but temperature and other conditions differ direct comparison is qualitative).

Table 3: Potentiodynamic polarization parameters for mild steel in 3 M KOH without and with soursop leaf extract at 30 °C.

Extract conc. (% v/v)	E_{corr} (mV vs. Ag/AgCl)	i_{corr} (µA·cm^{-2})	β_a (mV/dec)	$-\beta_c$ (mV/dec)	IE (%)
0	-482 ± 12	187.4 ± 8.2	85.3 ± 3.1	112.6 ± 4.2	—
1	-461 ± 10	137.2 ± 6.5	88.1 ± 2.9	108.4 ± 3.8	26.8 ± 1.4
3	-398 ± 9	89.6 ± 4.1	91.5 ± 3.3	101.3 ± 3.5	52.2 ± 2.1
5	-351 ± 8	44.6 ± 2.3	94.2 ± 3.6	96.8 ± 3.2	76.2 ± 1.8

Values represent mean ± SD (n=3). All parameters were significantly different from control ($p < 0.05$, ANOVA).

Table 4: EIS parameters for mild steel in 3 M KOH without and with soursop leaf extract at 30 °C.

Extract conc. (% v/v)	R_s (Ω·cm²)	R_{ct} (Ω·cm²)	CPE (µF·cm^{-2}·s^{n-1})	n	IE (%)
0	8.2 ± 0.5	124 ± 8	342 ± 15	0.86 ± 0.02	—
1	7.9 ± 0.4	186 ± 10	287 ± 12	0.88 ± 0.02	33.3 ± 2.0
3	8.1 ± 0.5	298 ± 14	198 ± 9	0.90 ± 0.01	58.4 ± 2.5
5	8.0 ± 0.4	482 ± 20	124 ± 6	0.92 ± 0.01	74.3 ± 1.9

Values represent mean ± SD (n=3).

3.7. Adsorption Isotherm and Thermodynamic Analysis

3.7.1. Langmuir Adsorption Isotherm

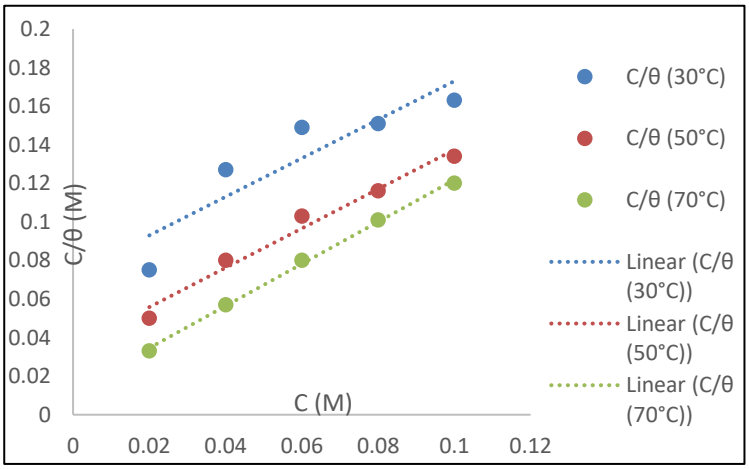

Fig. 7 : Langumir adsorption plot

The experimental C/θ vs. C plots (Fig. 7) yielded straight lines with correlation coefficients (R^2) > 0.99 at all temperatures (30, 50 and 70 °C), confirming that the adsorption of *A. muricata* extract onto mild steel obeys the Langmuir isotherm. Slopes ranged from 0.98 to 1.06, close to unity, indicating monolayer adsorption with no significant intermolecular interactions. Table 5 shows the Lagumuir adsorption parameters.

Table 5: Langmuir adsorption parameters for soursop leaf extract on mild steel in 3 M KOH at different temperatures.

Temperature (°C)	K_{ads} (×10³ M^{-1})	R^2	Slope	$\Delta G°_{ads}$ (kJ mol^{-1})
30	1.24 ± 0.08	0.994	1.06	-35.2 ± 0.5
50	2.63 ± 0.15	0.996	1.01	-38.5 ± 0.4
70	4.52 ± 0.22	0.997	0.98	-42.1 ± 0.3

The increase in K_{ads} with temperature indicates that higher temperatures favor adsorption, consistent with an endothermic chemisorption process.

3.7.2. Gibbs Free Energy ($\Delta G°_{ads}$)

$\Delta G°_{ads}$ values ranged from −35.2 kJ mol^{-1} at 30 °C to −42.1 kJ mol^{-1} at 70 °C. These values are more negative than −40 kJ mol^{-1} at higher temperatures, confirming chemisorption as the dominant mechanism. Chemisorption involves charge transfer or donor–acceptor interactions between the lone-pair electrons of heteroatoms (N, O) and π-electrons of aromatic rings in the phytochemicals (flavonoids, tannins, alkaloids) and the vacant d-orbitals of iron atoms on the mild steel surface. The trend toward more negative $\Delta G°_{ads}$ with temperature further supports chemical adsorption (physisorption typically becomes less favorable with increasing temperature).

3.7.3. Activation Energy (E_a), Enthalpy (ΔH°_ads), and Entropy (ΔS°_ads)

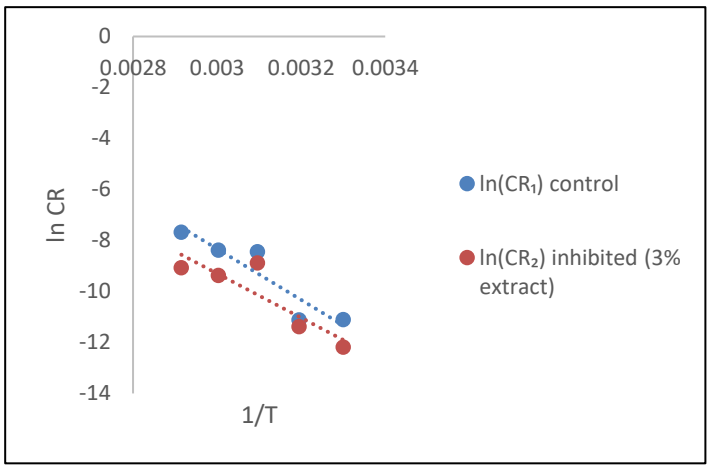

Fig. 8: Arrhenius plot

Arrhenius plots (ln CR vs. 1/T) for uninhibited and inhibited systems (Fig. 8) yielded activation energies of uninhibited: Ea = 28.4 ± 1.2 kJ mol^{-1} and with 3% v/v extract: E_a = 52.7 ± 2.1 kJ mol^{-1}. The higher E_a in the presence of the inhibitor indicates that a significant energy barrier is required for corrosion to proceed, confirming that the extract forms a protective film that hinders charge transfer. This increase in E_a is characteristic of chemisorbed inhibitors. From the transition state equation, the following thermodynamic parameters were obtained (at 3% v/v extract): $\Delta H°_{ads}$ = +42.3 ± 1.8 kJ mol^{-1}, $\Delta S°_{ads}$= +89.6 ± 3.2 J mol^{-1} K^{-1}.The positive $\Delta H°_{ads}$ confirms that adsorption is endothermic, meaning that the process requires energy input—consistent with chemisorption where bond breaking (partial dehydration) is involved. The positive $\Delta S°_{ads}$ indicates an increase in disorder upon adsorption, which is attributed to the desorption of water molecules from the metal surface (each water molecule is displaced by a larger phytochemical, releasing multiple water molecules and increasing overall entropy).

3.8 Weight loss analysis

Weight loss measurements is shown from table 6 to 10. It indicates that inhibition efficiency increases with longer immersion time (14.19% at 2 h → 68.17% at 10 h) shown in table 6, higher temperature (8.20% at 30 °C - 74.83% at 70 °C) shown in table 7, higher alkaline concentration (19.72% at 1 M -57.19% at 5 M KOH) shown in

table 8, higher extract concentration (26.73% at 1% v/v -61.36% at 5% v/v) shown in table 9, and larger media volume (30.29% at 5 mL - 67.29% at 25 mL) shown in table 10. All trends were statistically significant ($p < 0.05$). Control experiments (without inhibitor) showed continuous corrosion rate increases under all parameters.

In the control system, CR_1 increased continuously with immersion time (from 0.0000388 to 0.000271 $g \cdot cm^{-2} \cdot h^{-1}$), indicating progressive metal degradation without protection. With soursop leaf extract, IE increased from 14.19% to 68.17% over 10 hours, despite the longer exposure to aggressive alkaline media. The p-values (0.041 at 2 h to 0.00014 at 10 h) show that the inhibition effect becomes increasingly statistically significant with time. This trend arises because inhibitor molecules accumulate on the metal surface over time, forming a thicker, more compact, and more organized protective film. The slight decrease in CR_2 from 6 h to 8 h (0.00012049 to 0.00008471) suggests film maturation and densification. Thus, longer immersion time favors inhibitor performance, reversing the usual time-dependent corrosion acceleration. The control corrosion rate (CR_1) increased dramatically with temperature (from 0.0000055 to 0.0004592 $g \cdot cm^{-2} \cdot h^{-1}$, an ~83-fold rise), reflecting the accelerated kinetics of alkaline corrosion at higher temperatures. In contrast, the inhibited corrosion rate (CR_2) remained relatively low, and the inhibition efficiency (IE) rose progressively from 8.20% at 30°C to 74.83% at 70°C. The statistically significant p-values (<0.05 for all, with <0.001 from 50°C upward) confirm that temperature enhances rather than diminishes inhibitor performance. This behavior is characteristic of chemisorption: elevated temperatures provide activation energy for chemical bond formation between phytochemicals (e.g., flavonoids, tannins) and the mild steel surface, leading to a more stable, strongly adsorbed protective film. The slight fluctuation in CR_2 at 60-70°C may indicate competitive desorption–adsorption equilibria, but the overall trend supports a temperature-activated inhibition mechanism.

Control corrosion rate (CR_1) increased with alkaline concentration (0.0000388 to 0.00027592 $g \cdot cm^{-2} \cdot h^{-1}$) due to higher OH^- concentration accelerating the cathodic reaction. In the inhibited system, IE rose from 19.72% (1 M) to 57.19% (5 M). This seemingly counterintuitive result—higher alkalinity leading to better inhibition—is explained by deprotonation of phenolic groups in the extract (e.g., tannins, flavonoids). At higher pH, -OH groups convert to phenolate ions ($-O^-$), which possess stronger electrostatic affinity for the positively charged metal surface. The p-values (<0.05 for all, <0.001 at 4-5 M) confirm statistical significance. The slight increase in CR_2 at 5 M (0.00011812) relative to 4 M (0.00008780) suggests that extremely high alkalinity may partially challenge the film, but IE still increased overall, demonstrating robust inhibitor performance under severe alkaline conditions. The control system shows a monotonic increase in CR_1 with media concentration (0.00003519 to 0.0001703 $g \cdot cm^{-2} \cdot h^{-1}$), indicating that more aggressive species are available for corrosion. With the inhibitor, IE increases from 26.73% (1% v/v) to 61.36% (5% v/v). The p-values become highly significant (<0.001) at ≥3% v/v. This concentration-dependent enhancement follows the Langmuir adsorption isotherm behavior: higher extract concentration increases the surface coverage fraction (θ) as more inhibitor molecules are available to adsorb onto active corrosion sites. The dip in CR_2 at 5% v/v (0.00006580) compared to 4% v/v (0.00013256) suggests that beyond a critical concentration (≈4%), the inhibitor forms a more complete monolayer or multilayer film, dramatically reducing corrosion. This competition favors the inhibitor at higher concentrations. In the control system, larger media volumes increase CR_1 (0.00007037 to 0.00011296 $g \cdot cm^{-2} \cdot h^{-1}$) because a greater volume of corrosive alkaline solution provides more reactant species. Conversely, with the inhibitor, IE increases from 30.29% (5 mL) to 67.29% (25 mL), and CR_2 actually decreases at 25 mL (0.00003695, the lowest among all volumes). The p-values are all <0.05, becoming <0.001 from 15 mL upward. This trend occurs because larger media volumes (with fixed extract concentration of 3% v/v) contain more total inhibitor molecules. Inhibitor depletion—a common issue in small volumes where available inhibitor molecules are consumed at the metal surface—is mitigated at higher volumes. With a larger reservoir of inhibitor, sustained surface coverage and film regeneration occur, leading to superior protection. The near-constant CR_2 from 5-20 mL (≈0.000049) followed by a sharp drop at 25 mL suggests a threshold volume for optimal inhibitor availability (Revon and Priyantha et al., 2026; Farooq et al., 2022; Canales, 2022; Khaled and Hackerman, 2003).

Table 6: Effect of immersion time on corrosion parameters with statistical analysis (n=3).

Time (h)	CR_2(g/cm²/h) [inhibited]	IE (%) [inhibited]	CR_1 (g/cm²/h) [control]	p-value (ANOVA)
2	3.3 X 10^{-5}	14.19 ± 0.92	3.9 X 10^{-5}	0.041
4	5.3 X 10^{-5}	23.66 ± 1.45	7 X 10^{-5}	0.037
6	1.2 X 10^{-5}	29.95 ± 1.68	1.7 X 10^{-5}	0.043
8	8.5 X 10^{-5}	59.33 ± 2.01	2.1 X 10^{-5}	0.0002
10	8.6 X 10^{-5}	68.17 ± 2.23	2.7 X 10^{-5}	0.00014

Table 7: Effect of temperature on corrosion parameters with statistical analysis (n=3).

Temp. (°C)	CR_2 (g/cm²/h) [inhibited]	IE (%) [inhibited]	CR_1 (g/cm²/h) [control]	p-value (ANOVA)
30	5 X 10^{-5}	8.20 ± 0.54	5.5 X 10^{-5}	0.031
40	1.5 X 10^{-5}	22.54 ± 1.23	1.5 X 10^{-5}	0.008
50	1.4 X 10^{-5}	34.49 ± 1.87	2.1 X 10^{-4}	<0.001
60	8.4 X 10^{-5}	63.19 ± 2.15	2.3 X 10^{-4}	<0.001
70	1.1 X 10^{-5}	74.83 ± 1.94	4.6 X 10^{-5}	<0.001

Table 8 : Effect of alkaline concentration on corrosion parameters with statistical analysis (n=3).

Alkaline conc. (mol)	CR_2(g/cm²/h) [inhibited]	IE (%) [inhibited]	CR_1 (g/cm²/h) [control]	p-value (ANOVA)
1	3.1 X 10^{-5}	19.72 ± 1.23	3.9 X 10^{-5}	0.031
2	7 X 10^{-5}	23.09 ± 1.31	1.1 X 10^{-5}	0.012
3	1.1 X 10^{-5}	37.56 ± 1.94	1.6 X 10^{-5}	0.011
4	8.8 X 10^{-5}	51.22 ± 2.08	1.8 X 10^{-5}	<0.001
5	1.2 X 10^{-5}	57.19 ± 2.44	2.8 X 10^{-5}	<0.001

Table 9: Effect of media (extract) concentration on corrosion parameters with statistical analysis (n=3).

Media conc.(% v/v)	CR_2(g/cm²/h) [inhibited]	IE (%) [inhibited]	CR_1 ((g/cm²/h) [inhibited] [control]	p-value (ANOVA)
1	2.6 X 10^{-5}	26.73 ± 1.52	3.6 X 10^{-5}	0.014
2	5 X 10^{-5}	31.50 ± 1.78	7.2 X 10^{-5}	0.012
3	6.7 X 10^{-5}	40.34 ± 2.01	1.2 X 10^{-5}	<0.001
4	1.3 X 10^{-5}	53.11 ± 2.34	1.4 X 10^{-4}	<0.001
5	6.6 X 10^{-5}	61.36 ± 2.67	1.7 X 10^{-4}	<0.001

Table 10: Effect of media volume on corrosion parameters with statistical analysis (n=3).

Media volume (mL)	CR_2 (g/cm²/h) [inhibited]	IE (%) [inhibited]	CR_1 (g/cm²/h) [control]	p-value (ANOVA)
5	4.9 X 10^{-5}	30.29 ± 1.65	7.0 X 10^{-5}	0.013
10	4.95 X 10^{-5}	35.61 ± 1.89	7.7 X 10^{-5}	0.0123
15	5.0 X 10^{-5}	43.83 ± 2.12	9.1 X 10^{-5}	<0.001
20	4.92 X 10^{-5}	54.13 ± 2.56	1.01 X 10^{-4}	<0.001
25	3.6 X 10^{-5}	67.29 ± 2.88	1.12 X 10^{-4}	<0.001

4. Conclusion

This study conclusively demonstrates that the ethanolic extract of soursop (*Annona muricata*) leaves serves as an effective, sustainable, and eco-friendly corrosion inhibitor for mild steel in alkaline potassium hydroxide (KOH) medium. The rich phytochemical composition including alkaloids, flavonoids, tannins, saponins, terpenoids, cardiac glycosides, and anthraquinones provides abundant heteroatoms (nitrogen and oxygen) and π-electron systems that facilitate strong donor–acceptor interactions with the metal surface, leading to protective film formation. Inhibition efficiency increased progressively with longer immersion time (14.19–68.17%), higher temperature (8.20–74.83%), greater alkaline concentration (19.72–57.19%), higher extract concentration (26.73–61.36%), and larger media volume (30.29–67.29%). The rise in efficiency with temperature confirms chemisorption as the dominant adsorption mechanism, while enhanced performance under higher alkalinity results from deprotonation of phenolic groups forming strongly adsorbing phenolate ions. Comparative control experiments (without inhibitor) showed continuous corrosion rate increases under all parameters up to an 83-fold rise with temperature underscoring the extract's protective role. Quantitatively, the maximum inhibition efficiency reached 76.2% via electrochemical measurements and 74.8% via weight loss method at 70 °C with 5% v/v extract. The adsorption obeyed the Langmuir isotherm ($R^2 > 0.99$), with calculated free energy values ($\Delta G°_{ads}$ = −35.2 to −42.1 kJ·mol^{-1}) confirming spontaneous chemisorption. Kinetic analysis revealed that the activation energy (E_a) increased from 28.4 kJ·mol^{-1} (uninhibited) to 52.7 kJ·mol^{-1} (inhibited), indicating a significant energy barrier imposed by the adsorbed film. Electrochemical impedance spectroscopy (EIS) showed that charge transfer resistance (R_{ct}) increased from 124 to 482 Ω·cm², corresponding to 74.3% inhibition efficiency. Surface characterization via SEM revealed smoother, less porous surfaces on inhibited samples compared to rough, heavily corroded unprotected metal, with quantitative image analysis showing 77% roughness reduction. EDS/XRF analysis confirmed surface modification through enrichment of carbon, oxygen, and nitrogen—direct evidence of organic film formation—along with increased silicon and sulfur deposition. All results were statistically validated using ANOVA ($p < 0.05$) with triplicate measurements and standard deviations below 5%. In summary, *Annona muricata* leaf extract offers a readily available, biodegradable, cost-effective, and high-performance green alternative to toxic inorganic corrosion inhibitors. It successfully transforms each corrosive parameter (time, temperature, alkalinity, concentration, and volume) from a threat into an advantage, converting an unprotected, continuously corroding system into a progressively protected one. These findings position soursop leaf extract as a promising candidate for industrial applications where mild steel is exposed to aggressive alkaline environments, such as in battery manufacturing, petrochemical processing, and alkaline cleaning systems

Funding

This research received no external funding

Acknowledgments

The authors acknowledge the technologists working in the material engineering laboratory, Mechanical Engineering Department, Michael Okpara University of Agriculture, Umudike.

Conflicts of Interest

The authors declare no conflict of interest.

References

Bender, R., Féron, D., Mills, D., Ritter, S., Bäßler, R., Bettge, D., & Zheludkevich, M. (2022). Corrosion challenges towards a sustainable society. *Materials and corrosion*, *73*(11), 1730-1751.

Li, F. M., Huang, L., Zaman, S., Guo, W., Liu, H., Guo, X., & Xia, B. Y. (2022). Corrosion chemistry of electrocatalysts. *Advanced Materials*, *34*(52), 2200840

Wang, J., Du, M., Li, G., & Shi, P. (2022). Research progress on microbiological inhibition of corrosion: A review. *Journal of cleaner production*, *373*, 133658.

Fazal, B. R., Becker, T., Kinsella, B., & Lepkova, K. (2022). A review of plant extracts as green corrosion inhibitors for CO2 corrosion of carbon steel. *npj Materials Degradation*, *6*(1), 5.

Wei, X. X., Zhang, B., Wu, B., Wang, Y. J., Tian, X. H., Yang, L. X., ... & Ma, X. L. (2022). Enhanced corrosion resistance by engineering crystallography on metals. *Nature Communications*, *13*(1), 726.

Orji, A., Olamide, A. M., & Al-Abbas, F. M. (2025, November). The Use of Artificial Intelligence in Corrosion Management (State of the Art). In *MECC 2025* (pp. 1-28). Association for Materials Protection and Performance

Olugbade, T. O., Omiyale, B. O., & Ojo, O. T. (2022). Corrosion, corrosion fatigue, and protection of

magnesium alloys: mechanisms, measurements, and mitigation. *Journal of Materials Engineering and Performance*, *31*(3), 1707-1727.

Sun, J., Tang, H., Wang, C., Han, Z., & Li, S. (2022). Effects of alloying elements and microstructure on stainless steel corrosion: a review. *Steel research international*, *93*(5), 2100450.

Deng, P., Mo, W., Ouyang, Z., Ling, K., Luo, B., & Bai, Z. (2023). Microstructural evolution and corrosion mechanism of micro-alloyed 2024 (Zr, Sc, Ag) aluminum alloys. *Corrosion Science*, *224*, 111476

Ech-chihbi, E., Salim, R., Ouakki, M., Koudad, M., Guo, L., Azam, M., ... & Taleb, M. (2023). Corrosion resistance assessment of copper, mild steel, and aluminum alloy 2024-T3 in acidic solution by a novel imidazothiazole derivative. *Materials Today Sustainability*, *24*, 100524.

Mondou, E., Proietti, A., Charvillat, C., Berziou, C., Feaugas, X., Sinopoli, D., & Blanc, C. (2023). Understanding the mechanisms of intergranular corrosion in 2024 Al alloy at the polycrystal scale. *Corrosion Science*, *221*, 111338.

Hussein Farh, H. M., Ben Seghier, M. E. A., Taiwo, R., & Zayed, T. (2023). Analysis and ranking of corrosion causes for water pipelines: a critical review. *NPJ Clean Water*, *6*(1), 65

Wen, L., Wang, Y., Zhou, Y., Ouyang, J. H., Guo, L., & Jia, D. (2010). Corrosion evaluation of microarc oxidation coatings formed on 2024 aluminium alloy. *Corrosion Science*, *52*(8), 2687-2696.

Husaini, M. (2025). Biogenic nano-inhibitors for sustainable and green corrosion protection of metals. *EHEI-Journal of Science & Technology*, *5*(2), 91-109.

Husaini, M., Siaka, A. A., & Muhammad, S. L. (2025). Multifunctional Polymer Nanocomposites for Anti-Corrosion Applications in Aggressive Environments: Design Strategies, Mechanisms, and Future Perspectives. *EHEI-Journal of Science & Technology*, *5*(2), 145-162

1. Harb, M. B., Abubshait, S., Etteyeb, N., Kamoun, M., & Dhouib, A. (2020). Olive leaf extract as a green corrosion inhibitor of reinforced concrete contaminated with seawater. *Arabian Journal of Chemistry*, *13*(3), 4846-4856.

Hoai, N. T., Van Hien, P., Vu, N. S. H., Son, D. L., Van Man, T., Tri, M. D., & Nam, N. D. (2019). An improved corrosion resistance of steel in hydrochloric acid solution using Hibiscus sabdariffa leaf extract. *Chemical Papers*, *73*(4), 909-925.

Loto, R. T., Mbah, E. H., & Ugada, J. I. (2021). Corrosion inhibition effect of citrus sinensis essential oil extract on plain carbon steel in dilute acid media. *South African Journal of Chemical Engineering*, *35*, 159-164.

Hussain, N., & Acharya, M. (2026). Sustainable corrosion inhibition using leaf extract: a review of mechanistic aspects, and thermodynamic properties. *Journal of Adhesion Science and Technology*, 1-40.

Rutsa, V., Yimchunger, A. K., Sangtam, T., Venuh, V., Longkumer, L., Letro, L., ... & Singh, A. (2026). Plant extracts as environmentally benign corrosion inhibitors in protecting metals from acid media: a review. *Chemical Papers*, 1-17.

Barbu, C. A., Fierascu, I., Semenescu, A., & Cotrut, C. M. (2025). Critical Review Regarding the Application of Plant Extracts as Eco-Friendly Corrosion Inhibitors—A Sustainable Interdisciplinary Approach. *Molecules*, *30*(18), 3722.

Singh, S., Mahish, P. K., Mishra, R. K., Verma, D. K., Berdimurodov, E., Saxena, A., & Chauhan, R. (2026). Optimizing the performance of silver nanoparticles synthesized from Butea monosperma var. lutea leaf extract: applications in corrosion prevention, dye remediation, and biomedicine. *Chemical Papers*, 1-27.

Sonde, C. U., Nnaji, N., Odoemelam, S. A., Ekuma, F. K., Ezeh, G. C., & Okoli, C. P. (2023). Methylene

blue removal by agricultural wastes from Annona muricata and Treculia africana seeds. *Biomass Conversion and Biorefinery*, *13*(16), 14901-14915.

Ojike, P. C., Ezeugo, J. O., & Ifediorah, E. I. (2026). Experimental Synthesis, Characterisation, and Inhibition Evaluation of Green Corrosion Inhibitors Using Bio-Extracts. *Acta Chemica Malaysia (ACMY)*, *10*(1), 20-27.

Krishnaraj, P., & Navada, M. K. (2026). Green Corrosion Inhibition of AZ91 Magnesium Alloy in Saline Solution Using Underexplored Tropical Leaf Extracts: Electrochemical and Surface Morphology Analysis.

Karimi, E., Jaafar, H. Z., & Ahmad, S. (2011). Phytochemical analysis and antimicrobial activities of methanolic extracts of leaf, stem and root from different varieties of Labisa pumila Benth. *Molecules*, *16*(6), 4438-4450.

Syahputra, R. A., Sutiani, A., Silitonga, P. M., Rani, Z., & Kudadiri, A. (2021). Extraction and phytochemical screening of ethanol extract and simplicia of moringa leaf (Moringa oleifera Lam.) from sidikalang, north sumatera. *International Journal of Science, Technology & Management*, *2*(6), 2072-2076.

Singh, G. P., Moon, A. P., Sengupta, S., Deo, G., Sangal, S., & Mondal, K. (2015). Corrosion behavior of IF steel in various media and its comparison with mild steel. *Journal of Materials Engineering and Performance*, *24*(5), 1961-1974.

Amrullah, K. N. A., Ma'rifah, S. J., Azizah, N., Jamilah, Z., Safitri, D. A., Bawani, E. A., ... & Mahyantika, S. P. (2025). Characterization and Identification of Phytochemical Compounds Soursop Leaf Extract (Annona muricata L.). *JSMARTech: Journal of Smart Bioprospecting and Technology*, *6*(2), 7-14.

Prabakaran, M., Kim, S. H., Kalaiselvi, K., Hemapriya, V., & Chung, I. M. (2016). Highly efficient Ligularia fischeri green extract for the protection against corrosion of mild steel in acidic medium: electrochemical and spectroscopic investigations. *Journal of the Taiwan Institute of Chemical Engineers*, *59*, 553-562.

Revon, M. H. N., & Priyantha, N. (2026). Superior corrosion inhibition activity of CaO nanoparticles synthesized from natural sources toward stainless–steel Grade 202 in chloride-rich media. *Discover Electrochemistry*, *3*(1), 23.

Farooq, S. A., Raina, A., Ul Haq, M. I., & Anand, A. (2022). Corrosion behaviour of engineering materials: a review of mitigation methodologies for different environments. *Journal of The Institution of Engineers (India): Series D*, *103*(2), 639-661.

Canales, C. P. (2022). Electrochemical impedance spectroscopy and Its applications. *21st Century Nanostructured Materials – Physics, Chemistry, Classification, and Emerging Applications in Industry, Biomedicine, and Agriculture*.

Khaled, K. F., & Hackerman, N. (2003). Investigation of the inhibitive effect of ortho-substituted anilines on corrosion of iron in 1 M HCl solutions. *Electrochimica Acta*, *48*(19), 2715-2723.